Applied Physics A (2018) 124:723
https://doi.org/10.1007/s00339-018-2141-0

Applied Physics A
Materials Science & Processing

Structural and magnetic properties of copper oxide films deposited by DC magnetron reactive sputtering

L. Radjehi[1] · A. Djelloul[1] · M. Bououdina[2] · R. Siab[3] · W. Tebib[3]

Received: 11 July 2018 / Accepted: 27 September 2018

Abstract
Copper oxide films have been successfully deposited onto glass/Si(100) substrates by DC reactive magnetron sputtering in Ar/O_2 gas mixtures, while varying oxygen flow rate. The obtained results based on the structure and magnetic properties are discussed. Depending on the oxygen flow rate, the films reveal different phases and morphologies of Cu_2O, Cu_4O_3 and CuO. In addition, the magnetic properties of the copper oxides thin films are found to be strongly influenced by the oxygen flow rate; the ferro–para transition is influenced by the formation/cancellation of point defects.

1 Introduction

The abundance of copper, low production costs and its non-toxicity have attracted much attention for the synthesis of p-type copper oxides semiconductors. According to its oxidation number (Cu^0, Cu^{1+} and Cu^{2+}), copper can be found in different oxides such as Cu_2O, Cu_4O_3 and CuO. A recent report in the literature has shown that different copper oxides exhibit high potential applications as energy conversion, storage, transparent displays [1], sensor arrays [2], photocatalysts [3] and invisible integrated circuits [4]. Each of the above phases has well-defined crystal structures that influence its magnetic properties. In addition, copper oxides have different magnetic properties that depend mainly on the copper–oxygen covalent bond. Both CuO and Cu_4O_3 have an antiferromagnetic ground state. However, Cu_2O is a diamagnetic p-type semiconductor material [5].

Copper oxides can be synthesized by several techniques such as successive ionic layer adsorption and reaction (SILAR) [6], thermal oxidation [1, 7], molecular beam epitaxy [8], chemical vapour deposition (CVD) [9], sol–gel [5] and DC or RF magnetron sputtering [5, 10]. Among them, DC magnetron sputtering is considered as low-cost deposition method with a high deposition rate, as well as can be easily scaled up for industrial applications [5].

Varying the growth conditions allows to deposit simultaneously the three copper oxide phases (Cu_2O, Cu_4O_3 and CuO) using DC magnetron sputtering. A physicochemical model for reactive magnetron sputtering of a metal target reveals that the deposition of coating layers depends on the surface chemical reaction, which is mainly related to different deposition conditions such as reactive gas flow and the power density at the target [11].

According to the previous studies reported in the literature, various techniques have been proposed to deposit Cu oxides under different experimental conditions, resulting in the formation of single- or multi-phased system, with different morphologies and thereby different properties. In this study, phase-oxygen map was established. Particular focus is devoted to varying the oxygen flow rate during deposition while keeping all the remaining experimental parameters fixed and study its effect on phase stability/transformation and phase composition, crystallinity and grains orientation, morphology and size of grains and then the evolution of magnetic behaviour and properties.

In this paper, the metal target used is pure copper (Cu), is sputtered under argon and reactive O_2 gas environment onto silicon and glass substrates by DC magnetron sputtering process. The aim of this research work consists on a comprehensive study of the influence of oxygen flow rate on structural and magnetic properties of the different copper oxide films using XRD, FESEM and vibrating sample magnetometer

✉ M. Bououdina
mboudina@gmail.com

[1] LASPI2A Laboratoire des Structures, Propriétés et Interactions Inter Atomiques, Khenchela University, 40000 Khenchela, Algeria

[2] Department of Physics, College of Science, University of Bahrain, PO Box 32038, Zallaq, Bahrain

[3] Laboratoire de Physicochimie des Matériaux (LPCM), El Tarf University, 36000 El Tarf, Algeria

Published online: 01 October 2018

(VSM). Several crystal structures (Cu_2O, Cu_4O_3 and CuO) were deposited with high crystallinity.

2 Experimental part

Copper oxide films were deposited by DC reactive magnetron sputtering of a copper target (200 mm diameter and 99.9% purity) onto glass and silicon (100) substrates, using an Alcatel SCM 600 sputtering system. Argon and oxygen were used as reactive gas mixture. The substrates were cleaned in acetone and ethanol before their introduction in the growth chamber. By introducing 40 sccm pure argon gas, the pressure reached 10^{-4} Pa. The oxygen flow rate has been varied between 16 and 30 sccm. The deposition parameters are listed in Table 1.

The structure of the films was studied by X-ray diffraction (XRD D8 advanced with $\lambda = 0.154056$ nm) using Cu K_α radiation in $\theta/2\theta$ mode. The morphology of the films was checked using field emission scanning electron microscope (FE-SEM Hitachi SU 8030). Magnetic measurements were performed using EV-7 VSM vibrating sample magnetometer in magnetic field ≤ 20 kOe.

3 Results and discussion

3.1 Structure and microstructure analyses

Figure 1 displays the XRD patterns of copper oxide thin films deposited onto glass substrate with different oxygen flow rates (16, 20, 25 and 30 sccm). Depending on the oxygen flow rate, the deposited films exhibit different copper oxide phases. When the oxygen flow rate is fixed at 16 sccm, pure Cu_2O phase has been formed, which is in agreement with JCPDS card # 1-1142. At 20 sccm oxygen flow rate, XRD pattern shows the presence of an intense peak close to 36.58°, which can be assigned to the (111) reflection the

Table 1 Conditions of copper oxide film deposition in DC reactive magnetron sputtering

Deposition parameters	Value
Electrical intensity	1 A
Substrate temperature	68 °C
Work pressure	0.5 Pa
Base pressure	1×10^{-5} mbar
Deposition time	40 min
Oxygen flow ratio	10, 16, 20, 25, 30 and 35 sccm
Argon flow ratio	50 sccm
Target–substrate distance	145 mm

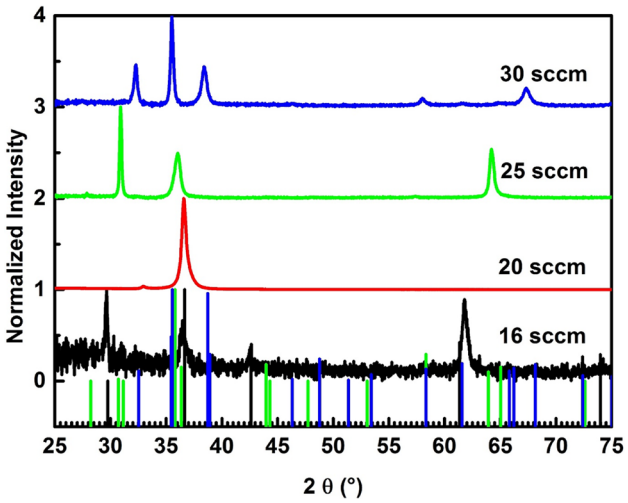

Fig. 1 XRD patterns of Cu_mO_n thin films with increasing oxygen flow rate. Black bar: JCPDS Card #1-1142 (Cu_2O), green bar: JCPDS card #49-1830 (Cu_4O_3), blue bar: JCPDS card #5-0661 (CuO)

cubic Cu_2O phase. In addition, a weak peak is observed at 32.52°, and is assigned to (110) reflection of the monoclinic structure CuO phase (JCPDS card # 5-0661). Thus, at this oxygen flow rate, the deposited film possesses two phases, namely Cu_2O and CuO. When the oxygen flow rate is set at 25 sccm, new diffraction peaks located at approximately 30.96°, 36.13° and 64.21° appear, which have been assigned to the (200), (004) and (400) reflections of the tetragonal structure Cu_4O_3 phase, in agreement with JCPDS card # 49-1830. Further increase in oxygen flow rate to 30 sccm leads to the disappearance of Cu_2O and Cu_4O_3 phases. Meanwhile, CuO phase (JCPDS # 5-0661) starts to emerge, with an intense diffraction peak (220) close to 35.4° and other weak peaks located at 32.52° (110), 38.73° (111), 58.34° (202) and 68.14° (220).

In the literature, the phase formation and composition are found dependent on the experimental conditions (synthesis route, precursors, post-treatment, etc.). Salavati-Niasari et al. [12] found that Cu with some amount of Cu_2O transformed into pure Cu_2O after controlled precipitation and dissolution of the previously prepared powder in C_6H_{12} and exposed to air. No other phases have been formed. Prabhakaran et al. [13] prepared pure Cu_2O phase with various morphologies by varying the temperature and reaction time (60 °C for 5 h, 60 °C for 6 h, 70 °C for 4 h and 80 °C for 4 h). It can be noticed that rare are studies reporting on Cu oxide phase formation/transformation while varying the experimental conditions. Zheng et al. [14] studied the phase formation, optical and electrical properties of Cu oxides. It was found the phase formation and phase composition are dependent on oxygen flow rate and total pressure inside the chamber: (1) pure phases of Cu_2O, Cu_4O_3, and CuO are formed at 0.5 Pa, while varying the oxygen flow rates at 8, 14, and 24

sccm; (2) further increase of oxygen flow rate up to 0.5 Pa, the following phase transformation/mixture occurred: $Cu_2O \rightarrow Cu_2O + Cu_4O_3 \rightarrow Cu_4O_3 + CuO \rightarrow CuO$; (3) at much high flow rate, the crystallinity of CuO deteriorated.

According to the literature, Cu oxide phase formation is dependent on oxygen partial pressure and oxidation state of Cu (Cu^+ and Cu^{2+}). According to the equilibrium phase diagram, only CuO (Cu^{2+}) and Cu_2O (Cu^+) phases are stable. However, in the literature, other metastable phases can be also formed: Cu_3O_2 (low temperature oxidation < 300 °C of copper can lead also to the formation of Cu_3O_2 phase before of CuO) [15], Cu_4O_3 (prepared by solvothermal method and is dependent on hydrate water content in the copper precursor $Cu(NO_3)_2$: symproportionation reaction ($2CuO + Cu_2O \rightarrow Cu_4O_3$) which is not feasible in aqueous media under mild synthesis conditions) [16] while no available experimental data are available for Cu_2O_3 phase, except computational study by density functional theory (DFT) on the small copper oxide clusters from Cu_2O to Cu_2O_4 as reported by Lai-Sheng Wang et al. (the authors studied the electronic structure of copper oxide clusters, Cu_2O_x ($x = 1$–4), using anion photoelectron spectroscopy and density functional calculations) [17]. In this study, the phase formation/transformation is found to be dependent on oxygen flow rate during the deposition process; both stable (Cu_2O and CuO) and metastable (Cu_4O_3 due to the presence of mixed Cu oxidation states $2Cu^+$ and $2Cu^{2+}$) phases are obtained.

Taking into consideration the as-obtained XRD results and the appearance of Cu_mO_n phases under various oxygen flow rate, the following general chemical reaction is regarded to take place:

$$Cu + \left(\frac{n}{2m}\right)O_2 \rightarrow \left(\frac{1}{m}\right)Cu_mO_n. \quad (1)$$

The reaction (1) occurs by the physical adsorption of O_2 molecules, which is described by the Langmuir isotherm adsorption model [11]. Using Eq. (1) and varying the number of moles of oxygen gas ($n/2m$), the evolution of different copper oxide phases as a function of the number of copper atoms (m) is shown in Fig. 2.

As a result, we can see that the copper oxide phases have been synthesized in this order: Cu_2O, Cu_3O_2, Cu_4O_3, CuO and Cu_2O_3. Knowing that Cu_2O and CuO are the most stable phases, the remaining phases are metastable and do not have a wide formation interval of oxygen flow rate.

Figure 3 shows FESEM images of Cu_mO_n deposited onto Si substrates at different oxygen flow rates. It is clearly evident that the morphology of the deposited films changes with oxygen flow rate. The films deposited at low oxygen flow rates (16 and 20 sccm) present homogenous spherical grains with different sizes from 58 to 90 nm. When the oxygen flow rate is equal to 25 sccm, the grain shape becomes elongated with grain size ranging from 50 to 70 nm. Furthermore, the

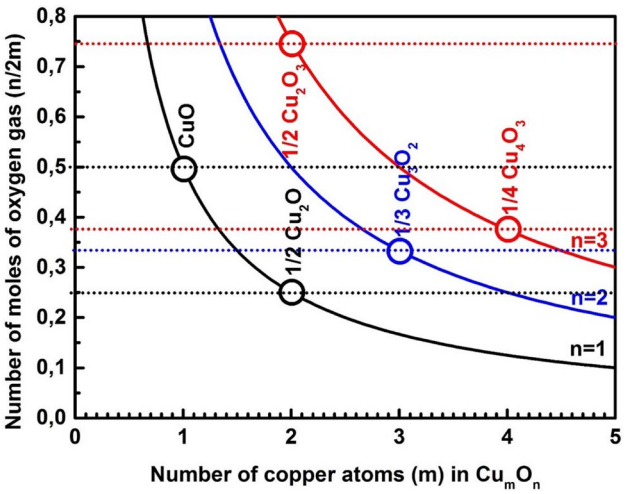

Fig. 2 FESEM images of copper oxide phases with increasing oxygen flow rate during the reactive sputtering process

film deposited at 30 sccm of oxygen flow rate shows columnar grains with a pyramid shape. The change in surface grain shape is related to the modification of microstructure as described in Fig. 1. Indeed, it was reported in several works that Cu_2O, Cu_4O_3 and CuO present spherical, elongated and pyramid surface grains, respectively [5]. The cross-sectional views of the deposited thin films show that all films present columnar morphology, which is related to the high working pressures (0.5–0.7 Pa). It is well-known that the mean free path of adatoms decreases with increasing working pressure, which leads to a decrease in the adatom surface mobility [18].

In the literature, it is well documented that the morphology of size of particles is strongly dependent on various parameters, starting from the preparation route, starting precursors and reagents, and experimental conditions and post-treatment (annealing). Prabhakaran et al. [13] reported the formation of octahedral, star/short hexapod and extended hexapod morphologies with onset/offset of oxidation temperatures of 304/551, 312/539, 400/525 °C, respectively. While Asar Ahmed et al. [19] found nano-octahedra (21–30 nm) Cu_2O phase by wet-chemical method using D-glucose and hydrazine as reducing agent at room temperature without the presence of any other surfactant. More recently, Thitinai Gaewdang et al. studied the effect of very slow oxygen flow rate (1–10 sccm) and argon flow rate of (12–32 sccm) on stability of CuO and Cu_2O phase thin films prepared by reactive magnetron sputtering under a pressure of 0.73 Pa [20]. It was found: (1) at 1 sccm, amorphous phase is formed with isolated particles; (2) at 2–4 sccm, Cu_2O phase is formed with pillar shaped particles ~ 31–33 nm; (3) at 6 sccm, CuO phase appeared with pillar shaped particles ~ 37 nm; (4) at 8 sccm, CuO phase with pyramidal shaped particles ~ 37 nm; and (5) surprisingly at 10 sccm, amorphous phase appeared

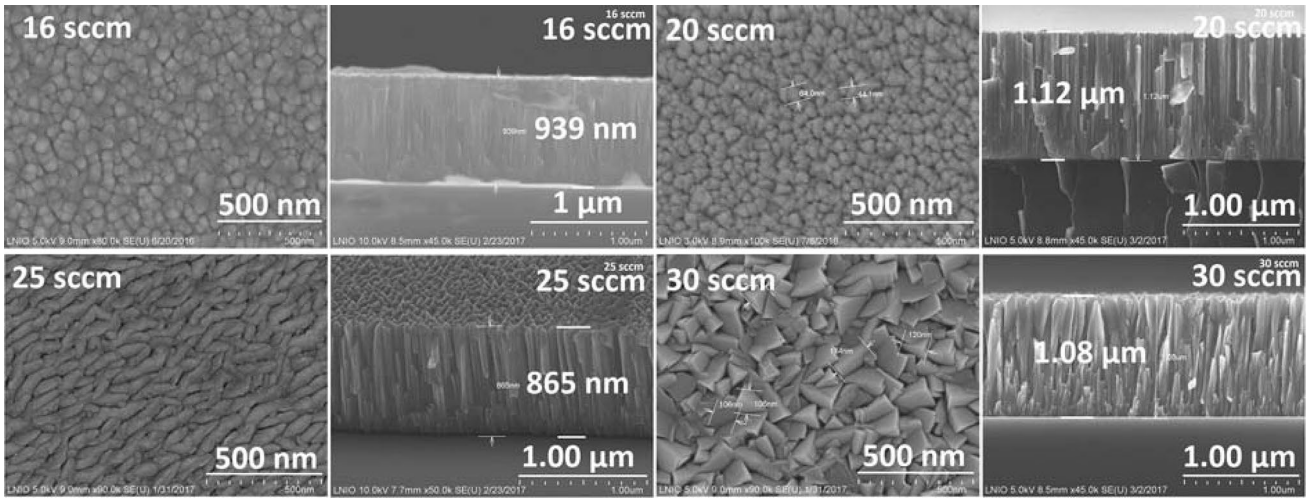

Fig. 3 FESEM images of the surface morphology and cross-sectional views of the deposited Cu_mO_n thin films

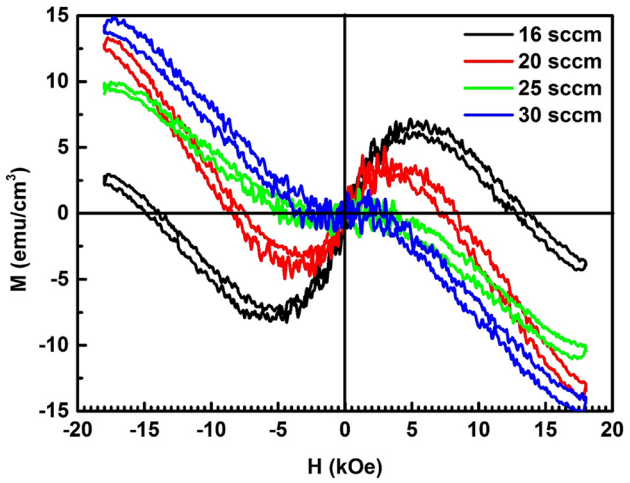

Fig. 4 Magnetization versus magnetic field (M–H) curves at room temperature for copper oxide thin films

again with flattered surface formed of particles with different shapes and sizes.

3.2 Magnetic properties

Figure 4 displays room temperature magnetization–field (M–H) curves of copper oxide thin films deposited under different oxygen flow rates. Diamagnetic contribution of glass substrate and sample holder has been subtracted from the recorded data. The values for magnetization (emu/cm^3) were calculated against the sample volume, estimated from the measured surface area of the sample and the film thickness determined by cross-sectional views of FESEM micrographs. It can be observed from Fig. 4 that the magnetic properties of copper oxide thin films are strongly influenced by the oxygen flow rate. The S-shaped form of the hysteresis loop indicates that the films deposited at 16 and 20 sccm of oxygen flow rate show a weak ferromagnetic behaviour alongside with diamagnetic component; whereas the films grown under 25 and 30 sccm reveal a dominant diamagnetic component alongside with a very weak ferromagnetic behaviour in the low field range. It is clear that with increasing the oxygen flow rate, the ferromagnetic behaviour reduces. This can be associated with the formation/disappearance of oxygen vacancies within copper oxide phases depending on atmosphere (air, hydrogen, vacuum) as previously observed experimentally and confirmed by first principle ab initio calculations using density functional theory (DFT) in other metal oxide semiconductors, CdO [21], ZnO [22] and MgO [23]. In copper oxide thin films deposited at 16 and 20 sccm, the saturation magnetizations (M_S) are ~ 7 and 3.75 emu/cm^3, namely, 0.03 μ_B and 0.016 μ_B per Cu_2O molecule in average, respectively.

According to the literature, the magnetic behaviour and properties are found to be sensitive to structural and microstructural parameters, including but not limited to the formed phase(s), phase composition, shape and size of particles, grains preferred orientation, point defects such as vacancies and/or interstitials, etc. It is known that Cu oxides are not magnetic in bulk even though Cu element has a magnetic moment in the range 1.7–2.2 μ_B; CuO is paramagnetic because Cu^{2+} has unpaired electron ([Ar] $3d^9$) while Cu_2O is diamagnetic because Cu+ has non-unpaired electron ([Ar] $3d^{10}$). Meanwhile, Prabhakaran et al. [12] observed room temperature ferromagnetism in Cu_2O nanoparticles due to quantum confinement at nanoscale regime, where the magnetic parameters varied slightly and were attributed to formation of oxygen vacancies and different morphologies (octahedral, star/short hexapod, extended

hexapod and microrod). On the other side, CuO nanoparticles with different morphologies (ellipsoidal to rodlike) and size (13–33 nm) were synthesized by thermal annealing of the copper hydroxide at various temperatures (150–550 °C). Accordingly, a weak ferromagnetic interaction and the blocking behaviour in these nanoparticles were observed [24]. Djurek et al. [25] studied the evolution of magnetic properties of Cu_4O_{3-x} ($x = 0.0$–0.5) nanoparticles (56 nm). The defect-free Cu_4O_3 is characterised by an inversion symmetry and exhibited both antiferromagnetic and ferromagnetic states, with a magnetic transition observed at low temperature ($T = 120$ K), probably as a result of an incommensurate ordering. Therefore, it can be highlighted that the study of magnetic behaviour as well as the evolution of magnetic properties of single-phase Cu oxides is quite complicated. Meanwhile, the investigation of the bulk magnetism for a Cu oxide multi-phased system remains very challenging and needs in-depth characterizations (TEM, AFM, XPS, SQUID, etc.) alongside with some computational calculations (DFT) to better understand the origin of magnetic ordering and changes in magnetic properties.

4 Conclusion

Highly transparent and conducting Cu_mO_n thin films have been grown by DC reactive magnetron sputtering in Ar–O_2 gas mixtures. XRD analysis confirms the presence of cubic, tetragonal and monoclinic structures of Cu_2O, Cu_4O_3 and CuO films, respectively. Surface morphology observations by FESEM reveal, spherical, elongated and columnar grains at the nanoscale regime for the different copper oxide phases. The magnetic properties are found strongly influenced by the oxygen flow rate, i.e. with increasing oxygen flow rate, the ferromagnetic behaviour degrades due to the formation/cancellation of oxygen vacancies.

References

1. H.A. Al-Jawhari, Mater. Sci. Semicond. Proc. **40**, 241–252 (2015)
2. C.L. Hsu, J.Y. Tsai, T.J. Hsueh, Sens. Actuators B Chem. **224**, 95–102 (2016)
3. H. Li, Z. Su, S. Hu, Y. Yan, App. Catal. B Environ. **207**, 134–142 (2017)
4. H. Sun, S.Ch. Chen, C.K. Wen, T.H. Chuang, M.A.P. Yazdi, F. Sanchette, A. Billard, Ceram. Int. **43**, 6214–6220 (2017)
5. A.S. Zoolfakar, R.A. Rani, A.J. Morfa, A.P. O'Mullaned, K. Kalantar-zadeh, J. Mater. Chem. C. **27**, 1–34 (2014)
6. Y. Wang, J. Ghanbaja, F. Soldera, S. Migot, P. Boulet, D. Horwat, F. Mücklich, J.F. Pierson, Appl. Surf. Sci. **335**, 85–91 (2015)
7. Y. Ievskaya, R.L.Z. Hoye, A. Sadhanala, K.P. Musselman, J.L. MacManus-Driscoll, Sol. Energy Mater. Sol. Cells **135**, 43–48 (2015)
8. M. Kracht, J. Schörmann, M. Eickhoff, J. Cryst. Growth **436**, 87–89 (2016)
9. J. Medina-Valtierra, C. Frausto-Reyes, G. Camarillo-Martınez, J.A. Ramırez-Ortiz, Appl. Catal. A Gen. **356**, 36–42 (2008)
10. A. Thobor, J.F. Pierson, Mater. Lett. **57**, 3676–3680 (2003)
11. V.I. Shapovalov, V.V. Karzin, A.S. Bondarenko, Phys. Lett. A **381**, 472–475 (2017)
12. M. Salavati-Niasari, F. Davar, Mater. Lett. **63**(3–4), 441–443
13. G. Prabhakaran, R. Murugan, J. Alloy. Compd. **579**, 572–575 (2013)
14. W. Zheng, Y. Chen, X. Peng, K. Zhong, Y. Lin, Z. Huang, Materials **11**, 1253 (2018). https://doi.org/10.3390/ma11071253, http://www.mdpi.com/journal/materials
15. M. Lenglet, K. Kartouni, J. Machefert, J.M. Claude, P. Steinmetz, E. Beauprez, J. Heinrich, N. Celati, Mater. Res. Bull. **30**(4), 393–403 (1995)
16. L. Zhao, H. Chen, Y. Wang, H. Che, P. Gunawan, Z. Zhong, H. Li, F. Su, Chem. Mater. **24**(6), 1136–1142 (2012)
17. L.-S. Wang, H. Wu, S.R. Desai, L. Lou, Phys. Rev. B **53**, 8028 (1996)
18. S. Achache, S. Lamri, A. Alhussein, A. Billard, M. François, F. Sanchette, Mater. Sci. Eng. **673**, 492–502 (2016)
19. A. Ahmed, N.S. Gajbhiye, A.G. Joshi, J. Solid State Chem. **184**, 2209–2214 (2011)
20. T. Gaewdang, N. Wongcharoen, IOP Conf. Ser. Mater. Sci. Eng. **211**, 012025 (2017)
21. M. Bououdina, A.A. Dakhel, M. El-Hilo, D.H. Anjum, M. Benali Kanoun, S. Goumri-Said, RSC Adv. **42**, 33233–33238 (2015)
22. A.A. Dakhel, M. Bououdina, A. Jaafar, W. Khan, S. Azam, J. Minar, M.B. Kanoun, S. Goumri-Said, J. Alloy. Compd. (2018). https://doi.org/10.1016/j.jallcom.2018.04.221
23. S. Azzaza, M. El-Hilo, S. Narayanan, J. Judith Vijaya, M. Bououdina, Mater. Chem. Phys. **143**, 1500–1507 (2014)
24. G. Narsinga Rao. Y.D. Yao, J.W. Chen, J. Appl. Phys. **105**, 093901 (2009). https://doi.org/10.1063/1.3120785
25. D. Djurek, M. Prester, D. Drobac, M. Ivanda, D. Vojta, J. Magn. Magn. Mater. **373**, 183–187 (2015)